Proton Cross-Sections from Heavy-Ion Data in Deep-Submicron Technologies

D. L. Hansen

***Abstract*—This paper reports on the calculation of proton SEU cross section from heavy-ion data using a number of different models. Model accuracy is checked using data on proton and heavy-ion cross sections from the published literature. The closed-form models developed with earlier semiconductor devices typically overestimated the proton cross section, and the difference increased with smaller feature sizes. The results emphasize that low LET heavy-ion data is crucial in determining the proton upset cross section.**

***Index Terms*—Heavy ion, prediction tool, proton induced SEU, SEU in deep submicron devices, SEU, single-event upset.**

I. Introduction

THE interaction of semiconductor devices with charged particles can result in corrupted data through a number of different single-event effects (SEE) that result from the creation of electron–hole pairs. In the case of heavy ions, these effects result through direct ionization caused by energy transfer between the incident ion and the semiconductor material. In the case of protons, the failures often result from indirect ionization, where the interaction between the incident proton and the semiconductor material causes a nuclear reaction and secondary products with a higher linear energy transfer (LET) than the incident proton create the ionized region.

Cyclotron testing is typically used to measure a device's sensitivity to SEE. However, the high cost of these tests has provided ample motivation for the development of a number of useful models for calculating the cross section of proton SEE from heavy-ion data [1]–[6]. In general, these SEE calculations are predicated on the use of proton–Si interaction models to determine the secondary products and the use of the heavy-ion data to determine the effect of the secondaries.

However, in recent years there have been a number of new developments that have had a profound effect on the accuracy of the models available. Current ASIC technologies boast feature sizes that are tens of nanometers wide. This provides something of a paradigm shift since now the track width of the incident heavy-ion is similar or greater in size than a single transistor. In addition, with these smaller feature sizes, it has become necessary to include the effects of direct ionization from protons [7][8]. Finally, the space radiation community now has the advantage of greater accessibility to improved nuclear-reaction cross sections through GEANT4 [9] based tools, including CREME-MC [10]. This has enabled greater fidelity in the modeling of nuclear reaction materials, which are external to the traditionally modeled sensitive volume [10].

This paper evaluates a number of models to determine their ability to calculate high-energy proton SEE cross sections of deep-submicrometer devices from heavy-ion data. While there have been a number of Monte Carlo based models developed previously [4]–[6], the focus of this paper is restricted to models generally available to the radiation community. Data provided in the open literature [11]–[32] is used to show that the older models underestimate the high-energy proton cross sections, and that the amount by which these models underestimate the proton cross section has increased as feature size has decreased. In contrast with appropriate selection of the threshold and saturated cross section, the CREME-MC tools can provide a reasonably reliable worst case estimate of the proton cross section, which can be important for mission upset-rate calculations.

II. Modeling and Data Collection

In order to develop a suitable data set for analysis, a number of papers in the open literature that include both proton and heavy-ion data were surveyed (Table I). The papers were published in the time frame from 2004–2013 and covered a number of different devices and operating modes, representing technology nodes from 45 to 220 nm. Proton energies used in SEE tests ranged from about 60 to 200 MeV. In cases where the data was not tabulated, the proton and heavy-ion data was digitized and placed into a database to facilitate automatic processing. In general, the analysis is limited to devices for which the upset cross section was measured on a "per bit" basis. Cases where there were significant numbers of "burst" errors, or single-event functional interrupts, were excluded.

Three models from the literature with closed-form equations were chosen. They were used to compare proton and heavy-ion cross-section data pulled from the literature. In the PROFIT model [1], the proton cross section (σ_p) is calculated based on the heavy-ion cross section ($\sigma_{\rm HI}$), the assumed charge collection depth (d), the density in numbers of Si atoms per cm^3 ($n =$ 5E22 atoms/cm^3), and the nuclear cross section for proton–Si interactions ($\sigma_{\rm nuc}$)

$$\sigma_p = nd(\sigma_{\rm HI})(\sigma_{\rm nuc}). \tag{1}$$

The modeling here follows the convention of the text, with a charge collection depth of 2 μm and assumes that all secondary products from the proton–Si interaction have the maximum LET (15 MeV cm^2/mg). In principle, this should provide an upper

Manuscript received July 14, 2015; revised September 03, 2015 and September 22, 2015; accepted September 23, 2015. Date of publication November 09, 2015; date of current version December 11, 2015.

The author is with Maxwell Technologies, Inc., San Diego, CA 92123 USA (e-mail: dhansen@maxwell.com).

Color versions of one or more of the figures in this paper are available online at http://ieeexplore.ieee.org.

Digital Object Identifier 10.1109/TNS.2015.2482360

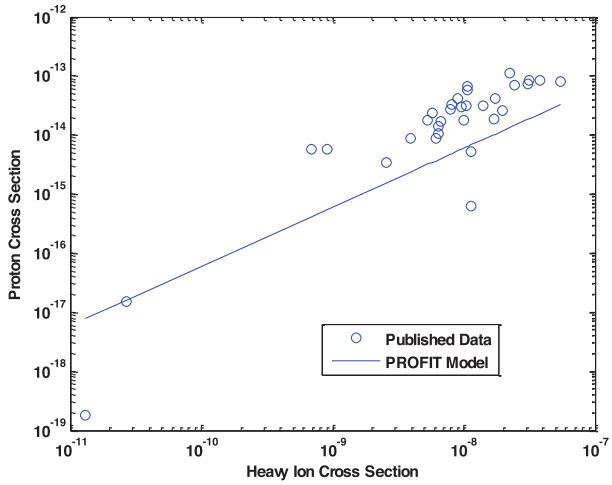

Fig. 1. Proton cross-section as a function of heavy-ion cross section at LET = 15 MeV cm^2/mg for the PROFIT model [1] and published data.

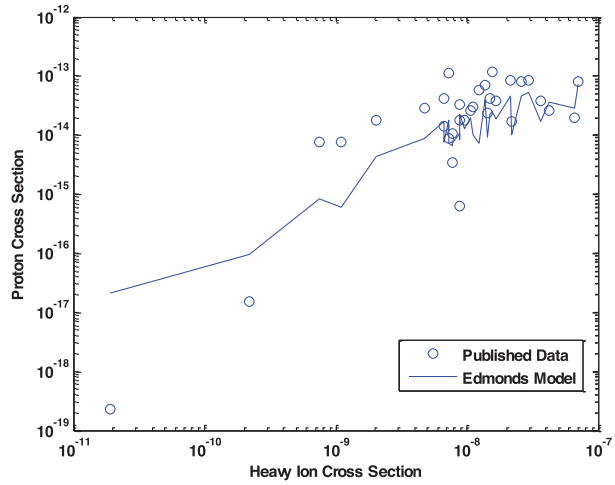

Fig. 2. Proton cross-section as a function of heavy-ion cross section at saturation ($\sigma_{\mathrm{HI}\infty}$). For the Edmonds model (2) [2] and published data.

TABLE I
FEATURE SIZE AND DEVICE TYPE OF DATA ANALYZED

Reference	Feature Size (nm)	Device Description
Koga [18]	220	UMC A54SX72A
Gadlage [13]	180	DFF 300MHz
Gadlage [13]	180	DICE 300MHz
Koga [17]	150	Virtex2 Config
Koga [17]	150	Virtex2 BRAM
Quinn [27]	150	Virtex II
Poivey [25]	130	SRAM
Cannon [11]	90	NAND2_1x
Cannon [11]	90	NAND2_2x
Cannon [11]	90	NOR2_1x
Cannon [11]	90	NOR2_2x
Cannon [12]	90	Commercial
Cannon [12]	90	RHBD B
Cannon [12]	90	RHBD C
George [15]	90	V4 SX55 BRAM
Lawrence [22]	90	Elpida 512 Mb SDRAM
Lawrence [23]	90	Node A SRAM
Lawrence [23]	90	Node B SRAM
Puchner [26]	90	QDRII SRAM
Swift [30]	90	Virtex4 BRAM55
Swift [30]	90	Virtex4 BRAM60
Swift [30]	90	Virtex4 BRAM200
Swift [30]	90	Virtex4 Config55
Swift [30]	90	Virtex4 Config60
Swift [30]	90	Virtex4 Config200
Heidel [16]	65	SOI 1.3V
Quinn [28]	65	Virtex5 XC5VLX50
Roche [29]	65	65nm no DNW
Roche [29]	65	65nm DNW
Sierawski [31]	65	SRAM
D'Alessio [32]	51	NAND Flash
Heidel [16]	45	SOI 1.2V

bound to the proton cross section since the typical nuclear fragment has LET $<$ 15 MeV cm^2/mg. We note, in most cases, the model underestimates the data (Fig. 1).

A likely cause of the PROFIT model's underestimation of the data arises from the fact that the expression used in that model for the nuclear interaction cross section is derived without taking into account pions, deutrons, tritons, He3, and alpha particles [38]. In small feature-size devices, sensitive to proton direct-ionization, these particles play a more significant role than in the larger devices used to validate this model.

The model proposed by Edmonds [2] assumes an exponential fit to the heavy-ion cross section and a number of assumptions about the proton cross section based on the rectangular parallelepiped (RPP) model frequently used in approximating charge-collection physics, as follows:

$$\sigma_p(E) = \sigma_{\mathrm{HI}\infty} \times \beta(E) \times \left(a \times L_{1/e}\right)^{-1}. \tag{2}$$

Here, a is a unit conversion between LET and liberated charge $[1.04\mathrm{E}-10\ \mathrm{C/cm(MeV\ cm^2/mg)^{-1}}]$, $L_{1/e}$ is the LET value where the cross section is 1/e times the saturated cross section, and β(E) is a function of energy given in the text of [2]. The saturated cross section ($\sigma_{\mathrm{HI}\infty}$) is taken from the heavy-ion upset data (Fig. 2). However, (2) is derived from an integral over the entire data set, given by

$$\sigma_p(E) = \beta(E) \times a^{-1} \int \sigma_{\mathrm{HI}} L^{-2} dL. \tag{3}$$

In this case, the cross-section calculation requires an integral over the full cross-section curve. For the modeling performed here, we used a linear fit of the log of the Weibull of the data with a threshold assumed to be 0.001 MeV cm^2/mg and a saturated cross section assumed to be 2$\times$ the maximum cross section measured, and only the data points up to LET = 10 MeV cm^2/mg were fit. These were assumed for simplicity of fitting and to emphasize the low LET data points. In fact, any method of fit could be used in the implementation of the data, and in fact, there may be several methods of fitting that provide better results.

With the Edmonds model implemented as described following (2), much of the charge collection information is lost, and the SEE sensitivity of the device at low LET is not accounted for adequately. In contrast, the implementation shown in (3) includes the low LET charge collection dynamics that are crucial to account for in devices that are sensitive to proton direct ionization. In fact, the low LET dynamics of the device are especially important because the proton cross section is dependent on the inverse square of the LET.

The model proposed by Barak *et al.* [3] is derived from the ratio of the figure of merit (FOM) equations presented by Petersen [33]. This model calculates the ratio of the proton and

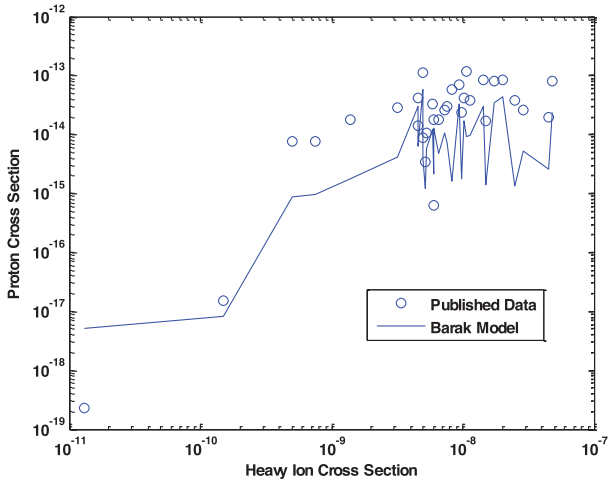

Fig. 3. Proton cross section as a function of heavy-ion cross section at saturation ($\sigma_{\mathrm{HI}\infty}$). The Barak model [3] is shown with the published data.

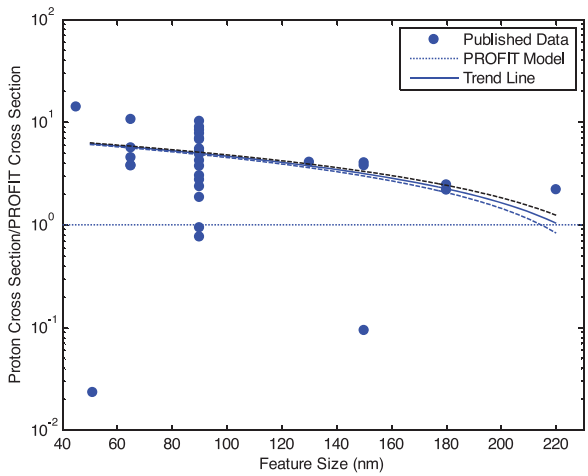

Fig. 4. Ratio of proton data to the predicted proton cross section for the PROFIT model [1] and published data. Trend line is calculated using the bootstrap method described in text. One standard deviation in the trend line slope is indicated by the dashed lines.

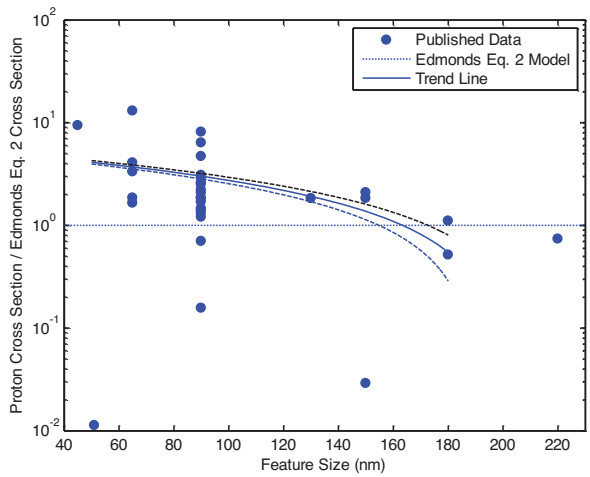

(a)

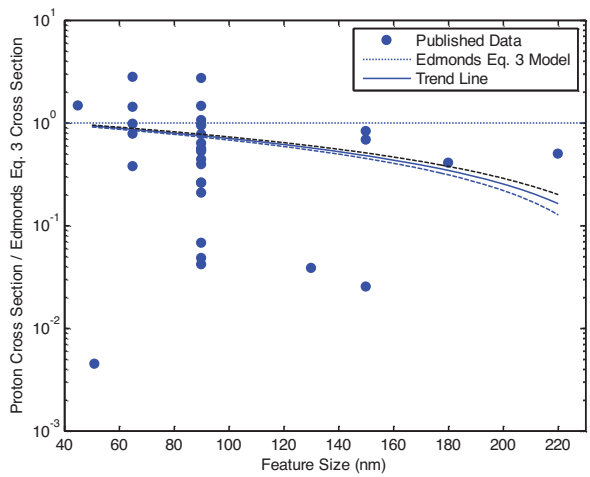

(b)

Fig. 5. Ratio of proton data to the predicted proton cross section for the Edmonds model in (a) Eq. (2), (b) Eq. (3) [2], and published data. Trend line is calculated using the bootstrap method described in text. One standard deviation in the trend line slope is indicated by the dashed lines.

heavy-ion saturated cross sections using the LET at 25% of the saturated cross section (L_{25})

$$\sigma_{p\infty}/\sigma_{\mathrm{HI}\infty} = 2.22 \cdot 10^{-5}(L_{25})^{-2} \tag{4}$$

where the ∞ subscript indicates the saturated cross section. As with the Edmonds model, one of the independent variables in calculating the proton cross section is the threshold LET. Consequently, when proton cross section is plotted as a function of heavy-ion cross section as in Figs. 2 and 3, the models do not appear monotonic. The Petersen FOM equations were derived empirically based on data from much older generation parts. Thus, we would only expect this model to accurately describe the proton cross sections of parts with charge collection characteristics that were similar to those used in deriving this model.

While all three models generally conform to the trend seen in the data, only Edmonds (3) does not typically underestimate the proton cross section, and typically the model is more likely to underestimate the data as the feature sizes get smaller. This can be seen more clearly by plotting the ratio of the measured and calculated cross-sections (Figs. 4–6).

In addition, the difference between the calculated and measured cross section tends to increase as the feature size decreases. This is not entirely surprising since these models were developed with much larger technologies, and even during their development it could be said that "even after a good track record has been established, (by a model) there is still some uncertainty as to whether a new case of interest will conform to the same pattern" [2].

The exception to this is the implementation of the Edmonds model using (3) (Fig. 5). For (3), the integral over the full heavy-ion cross section curve better accounts for the charge collection dynamics, and the use of the low LET heavy-ion cross section regime takes into account the additional effects of proton direct ionization which are more prevalent in the smaller feature devices. This model is dependent on the inverse square of the LET, and thus the heavy-ion cross section data at the lowest LETs drives the proton cross sections calculated. This is important to note since the low LET heavy-ion data is the most

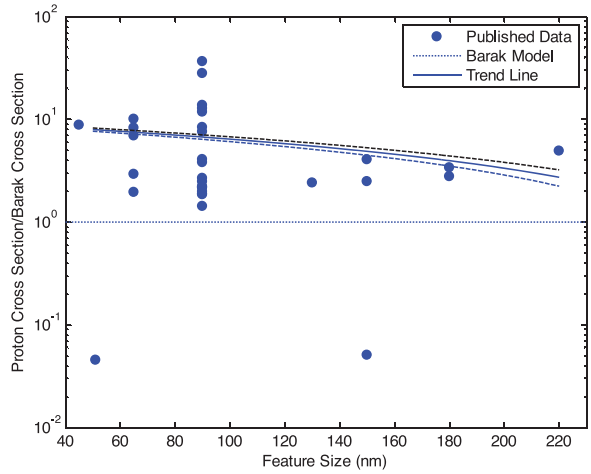

Fig. 6. Ratio of proton data to the predicted proton cross section for the Barak model [3] is shown with the published data. Trend line is calculated using the bootstrap method described in text. One standard deviation in the trend line slope is indicated by the dashed lines.

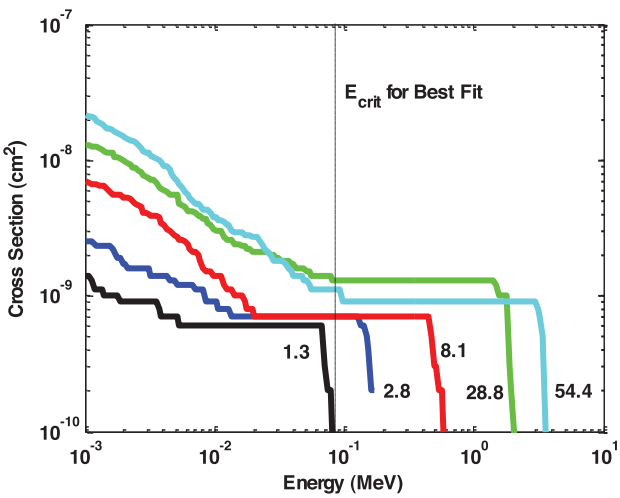

Fig. 7. Cross section curves generated by CREME-MC. Numbers indicate LET values. Vertical line indicates Ecrit used to obtain the fit to the heavy ion data. Numbers represent the LET values for each curve.

difficult to collect and is often limited because of the available experimental time.

In order to ensure that the trends observed are not merely the result of a few extreme points, a bootstrap analysis was used for verification. The bootstrap analysis was performed by randomly sampling with replacement from the original dataset to get an approximating dataset, which in practice will omit some data points while selecting other data points multiple times. For the analysis shown here, 1000 approximating datasets were created, and a linear fit was applied to each of them. From these linear fits, the average and standard deviation was calculated for the slope and the intercept. These were used to plot the trend lines in Figs. 4–6.

III. Modeling with CREME-MC

The CREME-MC suite of tools allows the user to perform Monte Carlo simulations of a variety of incident particles upon a sensitive volume modeled by a single or a group of RPPs. While this model does not have the simplicity of a closed-form equation, as was the case with the previous models, it is widely available to the radiation community on the Web [35].

Part of the power of CREME-MC arises from the fact that it allows the user to input a number of different parameters based on the physical operation of the device. These would include multiple sensitive volumes with adjustable charge-collection efficiencies and size [31], [34], [36], a variable "stack" to allow for different materials in the layers of the device [10], as well as the critical charge for the device.

The modeling performed here uses a simplified approach in that all parameters are derived from the SEE data without the benefit of TCAD modeling. The sensitive volume is a single RPP box. While this may be less physically correct than the multiple sensitive volumes which can be used in CREME-MC modeling, it has the advantage of simplicity, speed of calculation, and the fact that it has been successfully applied in many cases to determine device response [37]. In addition, the stack used is a single box comprised entirely of Si. This simplification is not unreasonable since it has been previously shown that in low threshold devices; the upset contribution from heavy metals is small relative to the Si contribution [5].

A. Selection of Parameter Definitions

In order to determine the most useful method for selecting the sensitive volume size and critical charge, a sensitivity analysis was developed by performing a number of CREME-MC runs using the dataset for the 45 nm device in [16]. The definition of LET threshold (L_{th}) and saturated cross section ($\sigma_{HI\infty}$) were changed in each run according to the values listed in Table II; thus, a total of 12 combinations were simulated. The initial estimate for critical charge in the simulations is derived from the heavy-ion data using the expression

$$E_{\text{crit}} = \rho \times L_{\text{th}} \times d \tag{4}$$

where ρ is the density of Si, and d is the charge collection depth. In these simulations, the expression $(\sigma_{HI\infty})^{1/2}$ provides the initial estimate of both the lateral dimensions of the sensitive volume as well as d. The heavy-ion data was then simulated in CREME-MC using the ions in Table III. The simulations were run in detailed mode with 10 000 particles and nuclear processes enabled. This generated the curves shown in Fig. 6. The best value for the critical energy from the CREME-MC plots in Fig. 7 is determined as the energy that minimizes the quantity

$$\sum_i \log\left(\left[\sigma_{\text{sim}}(i) - \sigma_{\text{data}}(i)\right]^2\right) \tag{5}$$

where $\sigma_{\text{data}}(i)$ and $\sigma_{\text{sim}}(i)$ represent the cross section for the data and simulation (respectively) at a specific energy for each of the LETs shown in Table III. Here, the *log* in the sum emphasizes the threshold region in the fit. Selecting the critical energy in this manner gives the cross section curve in Fig. 8.

Simulating the irradiation of the device with protons and using the critical energy values determined from the heavy-ion simulations shows which definition of L_{th} and σ_{SAT} provides the best values for use in calculating the proton cross section. Fig. 9 shows the ratio of the measured proton cross section at 63 MeV in [16] to the cross section calculated using CREME-MC for each of the conditions. The simulated proton

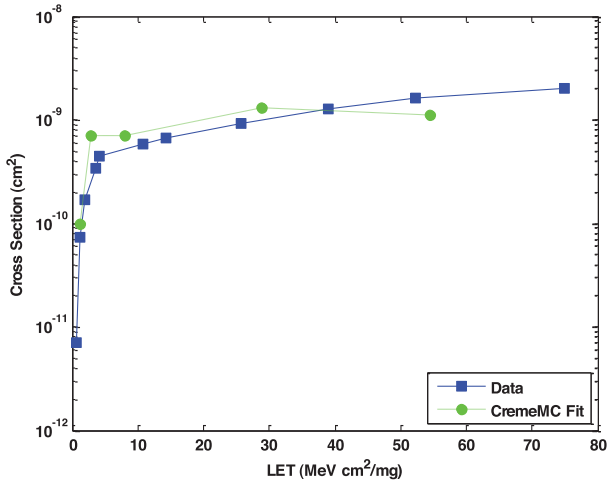

Fig. 8. Data from [16] and fit to data using CREME-MC curves in Fig. 7.

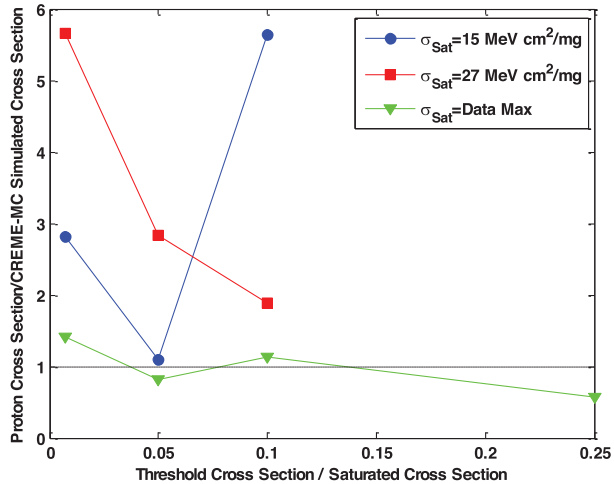

Fig. 9. Ratio of measured proton cross-section to simulated cross section as a function of the L_{th} definition for each of the σ_{SAT} definitions in Table II.

TABLE II
THRESHOLD AND SATURATED CROSS-SECTION DEFINITIONS USED IN CREME-MC SIMULATIONS

Parameter	Symbol	Value
L_{th}	L_{min}	LET at data minimum
L_{th}	L_5	LET at 5% σ_{SAT}
L_{th}	L_{10}	LET at 10% σ_{SAT}
L_{th}	L_{25}	LET at 25% σ_{SAT}
$\sigma_{HI\infty}$	σ_{15}	$\sigma_{HI\infty}$=σ at LET=15 MeV cm²/mg
$\sigma_{HI\infty}$	σ_{27}	$\sigma_{HI\infty}$= σ at LET=27 MeV cm²/mg
$\sigma_{HI\infty}$	σ_{max}	$\sigma_{HI\infty}$= σ at data maximum

TABLE III
IONS USED IN CREME-MC SIMULATIONS

Ion	Energy (MeV)	LET (MeV cm²/mg)
N	210	1.3
Ne	300	2.8
Ar	600	8.1
Kr	1260	28.8
Xe	1980	54.4

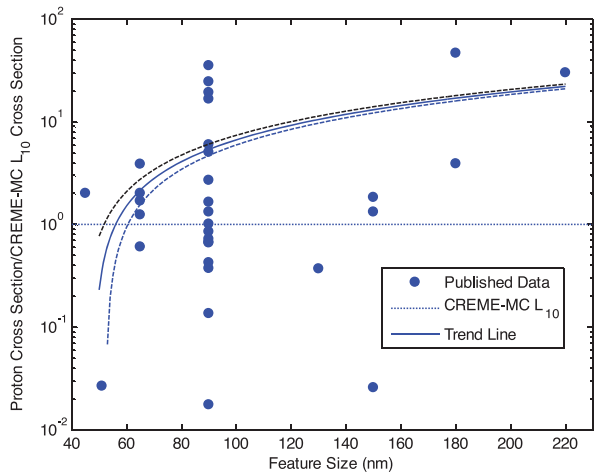

Fig. 10. Ratio of the proton data to the predicted proton cross section for the CREME-MC model using $L_{th} = L_{10}$. Trend line is calculated using the bootstrap method described in text. One standard deviation in the trend line slope is indicated by the dashed lines.

cross sections were calculated in "simplified" mode, with 1×10^6 particles.

There are a number of trends to note in Fig. 9. First for the σ_{15} and σ_{27} plots, there are no data points for the L_{25} value. This results from the fact that L_{25} represents the largest value for the critical energy (requiring more charge to upset the device) and the smallest size for the sensitive volume (limiting ions to a shorter track length). As a result, CREME-MC predicts sufficient charge will not be generated by the incident protons and no upsets will occur in these cases. This is clearly an incorrect result. In contrast, the cross-section values are most consistently predicted accurately by assuming the saturated cross section is the maximum of the data. Over all values of L_{th} used, the worst prediction is with 45% of the data (L_{25}), while the best is within 13% (L_{10}).

B. CREME-MC Simulation of Literature Data

Based on the results from the sensitivity analysis, the proton cross sections were run using σ_{max} to determine the sensitive volume size, with either L_{10} (Fig. 10) or L_{min} (Fig. 11) used to determine the critical charge. For the study of the literature data, the heavy-ion data was not simulated in CREME-MC. In both applications of the CREME-MC model, the data no longer shows the trend of greater underestimation of the data by the model and data as feature size decreases.

It should be noted that in using σ_{max} and L_{min} for modeling, the parameters are based, at least in part, on the choices of the experimenter in collecting data, rather than being a direct physical reflection of either the critical charge, or the saturated cross section. However, because the data was pulled from the literature, it might be safe to say that, on average, the σ_{max} and L_{min} values represent the "conventional wisdom" of the radiation community.

In order to compare the results (Fig. 12) for the different models, we look at a histogram of the data from Figs. 4–6 and Figs. 10–11. In Fig. 12, the horizontal axis represents the quantity

$$x = \log\left[\sigma_p\,(\text{data})\,/\sigma_p\,(\text{model})\right]. \tag{6}$$

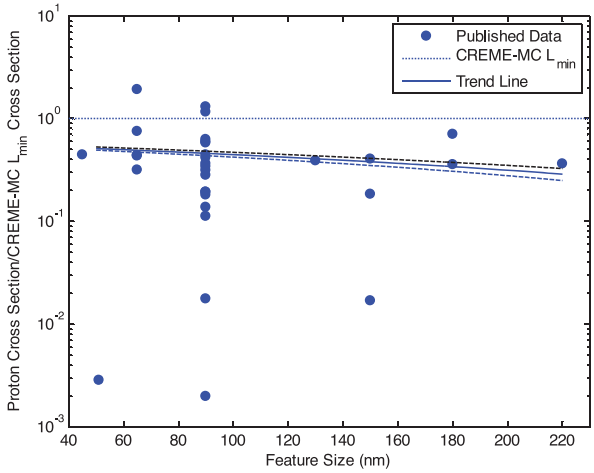

Fig. 11. Ratio of the proton data to the predicted proton cross section for the CREME-MC model using $L_{th} = L_{min}$. Trend line is calculated using the bootstrap method described in text. One standard deviation in the trend line slope is indicated by the dashed lines.

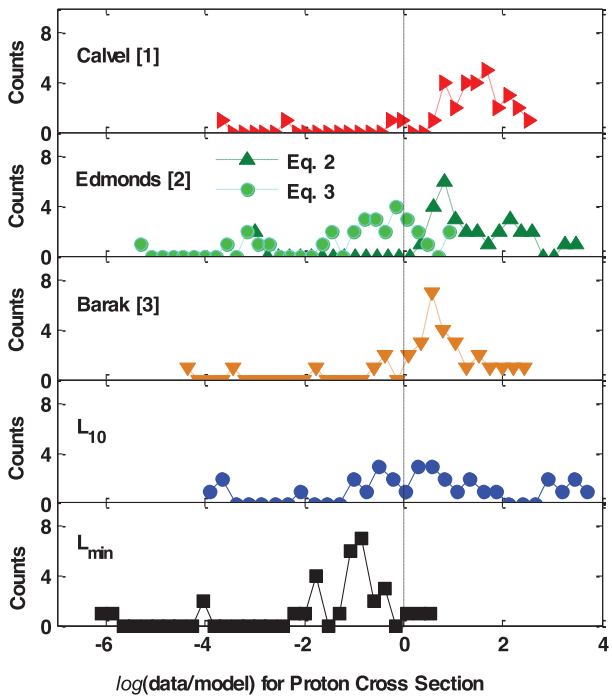

Fig. 12. Histogram of the data from Figs. 4–6 and Figs. 10–11. The vertical dashed line indicates agreement between model and data.

The dashed vertical line at $x = 0$ (Fig. 12) represents the point where $\sigma_p(\text{data}) = \sigma_p(\text{model})$. The vertical axis is the number of data points in each of the histogram "bins". The mean and median for the data in Fig. 12 is given in Table IV.

For all models used, there are outlier points where the models can be more than an order of magnitude different from the data. On average (Table IV), the CREME-MC L_{10} and Edmonds [2] models were the most accurate; however, it is interesting to note that the Edmonds' (3) and CREME-MC L_{min} model typically provided an upper bound for the proton cross section. This can be particularly useful in cases such as experimental planning or in mission assurance where an upper-bound estimate of an upset

TABLE IV
COMPARISON OF MODEL RESULTS

Model	log [σ_p(data) / σ_p(model)]	
	Mean	Median
Calvel [1]	1.1	1.4
Edmonds [2] Eq.2	0.41	0.61
Edmonds [2] Eq.3	-0.97	-0.6
Barak [3]	1.2	1.1
CREME-MC L_{10}	0.40	0.39
CREME-MC L_{min}	-1.4	-1.0

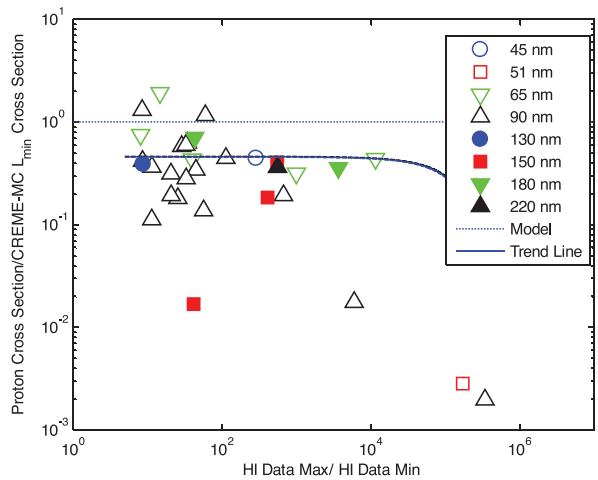

Fig. 13. Data from Fig. 11 plotted as a function of the ratio of $\sigma_{max}/\sigma_{min}$–data indicates that as you increase dynamic range you increase chance of overestimating proton cross section. Trend line is calculated using the bootstrap method described in text. One standard deviation in the trend line slope is indicated by the dashed lines.

cross section may be sufficient for worst-case analysis of SEE for the application.

To examine this further, if we plot the data from Fig. 11 as a function of $\sigma_{max}/\sigma_{min}$, where σ_{min} is the minimum cross section measured in the dataset, we see an interesting trend (Fig. 13). We note that the cases where the model underestimates the cross section are exclusively in the region where the data covers a smaller range of cross sections ($\sigma_{max}/\sigma_{min}$). Thus, in cases where an upper bound is sufficient for mission purposes, collection of the data such that $\sigma_{max}/\sigma_{min} \geq 100$ is likely adequate in the absence of TCAD modeling. The trend line in Fig. 13 suggests that increasing the data range further does not necessarily increase the accuracy of the modeled value. Further, just as the older models may not accurately predict the cross section of the newer technologies, the newer CREME-MC model may not accurately predict the proton cross section if it is implemented with the old "conventional wisdom" definition of LET threshold as the LET where the cross section as 10% of saturation. In both the CREME-MC modeling and the use of the Edmonds' model from (3), the importance of the heavy-ion data in the low LET regime is paramount.

IV. CONCLUSION

Using data from the literature on a number of deep submicrometer devices, we compared the effectiveness of a number

of different models in predicting proton cross section based on heavy-ion data. The closed-form models developed with earlier semiconductor devices typically overestimated the proton cross section. The exception was the Edmonds' model implemented using (3). The CREME-MC models used were accurate and able to produce an upper bound estimate of the proton cross section. However, in all cases, the low LET heavy-ion data was crucial in determining the proton upset cross section.

REFERENCES

[1] P. Calvel, C. Barillot, P. Lamothe, R. Ecoffet, S. Duzellier, and D. Falguere, "An empirical model for predicting proton induced upset," *IEEE Trans. Nucl. Sci.*, vol. 43, no. 6, pp. 2827–2832, Dec. 1996.

[2] L. D. Edmonds, "Proton SEU cross sections derived from heavy-ion test data," *IEEE Trans. Nucl. Sci.*, vol. 47, no. 5, pp. 1713–1728, Oct. 2000.

[3] J. Barak, "Simple calculations of proton SEU cross sections from heavy ion cross sections," *IEEE Trans. Nucl. Sci.*, vol. 53, no. 6, pp. 3336–3342, Dec. 2006.

[4] C. Weulersse, G. Hubert, G. Forget, N. Buard, T. Carriere, P. Heins, J. M. Palau, F. Saigne, and R. Gaillard, "DASIE analytical version: A predictive tool for neutrons, protons and heavy ions induced SEU cross section," *IEEE Trans. Nucl. Sci.*, vol. 53, no. 4, pp. 1876–1882, Aug. 2006.

[5] C. Inguimbert, S. Duzellier, T. Nuns, and F. Bezerra, "Using subthreshold heavy ion upset cross section to calculate proton sensitivity," *IEEE Trans. Nucl. Sci.*, vol. 54, no. 6, pp. 2394–2399, Dec. 2007.

[6] C. Weulersse, F. Wrobel, F. Miller, T. Carriere, R. Gaillard, J.-R. Vaille, and N. Buard, "A monte-carlo engineer tool for the prediction of SEU proton cross section from heavy ion data," in *Proc. 2011 Proc. 12th Eur. Conf. Radiat. Effects Compon. Syst.*, pp. 376–383.

[7] K. P. Rodbell, D. F. Heidel, H. H. K. Tang, M. S. Gordon, P. Oldiges, and C. E. Murray, "Low-energy proton-induced single-event-upsets in 65 nm node, silicon-on-insulator, latches and memory cells," *IEEE Trans. Nucl. Sci.*, vol. 54, no. 6, pp. 2474–2479, Dec. 2007.

[8] D. F. Heidel, P. W. Marshall, K. A. LaBel, J. R. Schwank, K. P. Rodbell, M. C. Hakey, M. D. Berg, P. E. Dodd, M. R. Friendlich, A. D. Phan, C. M. Seidleck, M. R. Shaneyfelt, and M. A. Xapsos, "Low energy proton single-event-upset test results on 65 nm SOI SRAM," *IEEE Trans. Nucl. Sci.*, vol. 55, no. 6, pp. 3394–3400, Dec. 2008.

[9] S. Agostinelli *et al.*, "Geant 4—A simulation toolkit," *Nucl. Instrum. Methods Phys. Rev. A*, vol. A506, pp. 250–303, 2003.

[10] K. M. Warren, R. A. Weller, M. H. Mendenhall, R. A. Reed, D. R. Ball, C. L. Howe, B. D. Olson, M. L. Alles, L. W. Massengill, R. D. Schrimpf, N. F. Haddad, S. E. Doyle, D. McMorrow, J. S. Melinger, and W. T. Lotshaw, "The contribution of nuclear reactions to heavy ion single event upset cross-section measurements in a high-density SEU hardened SRAM," *IEEE Trans. Nucl. Sci.*, vol. 52, no. 6, pp. 2125–2131, Dec. 2005.

[11] E. H. Cannon and M. Cabanas-Holmen, "Heavy ion and high energy proton-induced single event transients in 90 nm inverter, NAND and NOR gates," *IEEE Trans. Nucl. Sci.*, vol. 56, no. 6, pp. 3511–3518, Dec. 2009.

[12] E. H. Cannon, M. Cabanas-Holmen, J. Wert, T. Amort, R. Brees, J. Koehn, B. Meaker, and E. Normand, "Heavy ion, high-energy, and low-energy proton SEE sensitivity of 90-nm RHBD SRAMs," *IEEE Trans. Nucl. Sci.*, vol. 57, no. 6, pp. 3493–3499, Dec. 2010.

[13] M. J. Gadlage, P. H. Eaton, J. M. Benedetto, and T. L. Turflinger, "Comparison of heavy ion and proton induced combinatorial and sequential logic error rates in a deep submicron process," *IEEE Trans. Nucl. Sci.*, vol. 52, no. 6, pp. 2120–2124, Dec. 2005.

[14] J. Benedetto, P. Eaton, K. Avery, D. Mavis, M. Gadlage, T. Turflinger, P. E. Dodd, and G. Vizkelethy, "Heavy ion-induced digital single-event transients in deep submicron processes," *IEEE Trans. Nucl. Sci.*, vol. 51, no. 6, pp. 3480–3485, Dec. 2004.

[15] J. George, R. Koga, O. Swift, G. Allen, C. Carmichael, and C. W. Tseng, "Single event upsets in xilinx virtex-4 FPGA devices," in *Proc. 2006 IEEE Radiat. Effects Data Workshop*, pp. 109–114.

[16] D. F. Heidel, P. W. Marshall, J. A. Pellish, K. P. Rodbell, K. A. LaBel, J. R. Schwank, S. E. Rauch, M. C. Hakey, M. D. Berg, C. M. Castaneda, P. E. Dodd, M. R. Friendlich, A. D. Phan, C. M. Seidleck, M. R. Shaneyfelt, and M. A. Xapsos, "Single-event upsets and multiple-bit upsets on a 45 nm SOI SRAM," *IEEE Trans. Nucl. Sci.*, vol. 56, no. 6, pp. 3499–3504, Dec. 2009.

[17] R. Koga, J. George, G. Swift, C. Yui, L. Edmonds, C. Carmichael, T. Langley, P. Murray, K. Lanes, and M. Napier, "Comparison of xilinx virtex-II FPGA SEE sensitivities to protons and heavy ions," *IEEE Trans. Nucl. Sci.*, vol. 51, no. 5, pp. 2825–2833, Oct. 2004.

[18] R. Koga, K. Crawford, P. Yu, J. George, S. Crain, M. Zakrzewski, and J. J. Wang, "Heavy ion and proton see characterization of COTS0.22 μm field programmable gate arrays," in *Proc. 2005 IEEE Radiat. Effects Data Workshop*, pp. 57–64.

[19] R. Koga, P. Yu, S. Crain, and J. George, "Proton and heavy ion induced semi-permanent upsets in double data rate SDRAMs," in *Proc. 2007 IEEE Radiat. Effects Data Workshop*, pp. 199–203.

[20] R. Koga, P. Yu, J. George, and S. Bielat, "Sensitivity of 2 Gb DDR2 SDRAMs to protons and heavy ions," in *Proc. 2010 IEEE Radiat. Effects Data Workshop*, pp. 17–22.

[21] R. Koga, J. George, and S. Bielat, "Single event effects sensitivity of DDR3 SDRAMs to protons and heavy ions," in *Proc. 2012 IEEE Radiat. Effects Data Workshop*, pp. 1–8.

[22] R. K. Lawrence, "Radiation characterization of 512 Mb SDRAMs," in *Proc. IEEE Radiat. Effects Data Workshop*, 2007, pp. 204–207, The feature size for this paper is assumed to be 90 nm.

[23] R. K. Lawrence and A. T. Kelly, "Single event effect induced multiple-cell upsets in a commercial 90 nm CMOS digital technology," *IEEE Trans. Nucl. Sci.*, vol. 55, no. 6, pp. 3367–3374, Dec. 2008.

[24] C. Poivey, M. Berg, M. Friendlich, H. Kim, D. Petrick, S. Stansberry, K. A. LaBel, C. Seidleck, A. Phan, and T. Irwin, "Single event effects (SEE) response of embedded power PCs in a xilinx virtex-4 FPGA for a space application," in *Proc. 2007 9th Eur. Conf. Radiat. Effects Compon. Syst.*, pp. 1–5.

[25] C. Poivey, M. Grandjean, and F.-X. Guerre, "Radiation characterization of microsemi ProASIC3 flash FPGA family," in *Proc. 2011 IEEE Radiat. Effects Data Workshop*, pp. 1–5.

[26] H. Puchner, J. Tausch, and R. Koga, "Proton-induced single event upsets in 90 nm technology high performance SRAM memories," in *Proc. 2011 IEEE Radiat. Effects Data Workshop*, pp. 1–3.

[27] H. Quinn, P. Graham, J. Krone, M. Caffrey, and S. Rezgui, "Radiation-induced multi-bit upsets in SRAM-based FPGAs," *IEEE Trans. Nucl. Sci.*, vol. 52, no. 6, pp. 2455–2461, Dec. 2005.

[28] H. Quinn, K. Morgan, P. Graham, J. Krone, and M. Caffrey, "Static proton and heavy ion testing of the xilinx virtex-5 device," in *Proc. 2007 IEEE Radiat. Effects Data Workshop*, pp. 177–184.

[29] P. Roche, G. Gasiot, S. Uznanski, J.-M. Daveau, J. Torras-Flaquer, S. Clerc, and R. Harboe-Sørensen, "A commercial 65 nm CMOS technology for space applications: Heavy ion, proton and gamma test results and modeling," *IEEE Trans. Nucl. Sci.*, vol. 57, no. 4, pp. 2079–2088, Aug. 2010.

[30] G. M. Swift, G. R. Allen, W. T. Chen, C. Carmichael, G. Miller, and J. S. ,George, "Static upset characteristics of the 90 nm virtex-4QV FPGAs," in *Proc. 2008 IEEE Radiat. Effects Data Workshop*, pp. 98–105.

[31] B. D. Sierawski, J. A. Pellish, R. A. Reed, R. D. Schrimpf, K. M. Warren, R. A. Weller, M. H. Mendenhall, J. D. Black, A. D. Tipton, M. A. Xapsos, R. C. Baumann, X. Deng, M. J. Campola, M. R. Friendlich, H. S. Kim, A. M. Phan, and C. M. Seidleck, "Impact of low-energy proton induced upsets on test methods and rate predictions," *IEEE Trans. Nucl. Sci.*, vol. 56, no. 6, pp. 3085–3092, Dec. 2009.

[32] M. D'Alessio, C. Poivey, D. Walter, K. Gruermann, F. Gliem, H. Schmidt, R. H. Sorensen, A. Keating, N. Fleurinck, K. Puimege, D. Gerrits, and P. Mathijs, "NAND flash memory in-flight data from PROBA-II spacecraft," in *Proc. 14th Eur. Conf. Radiat. Effects Compon. Syst.*, 2013, pp. 1–6.

[33] E. L. Petersen, "The SEU figure of merit and proton upset rate calculations," *IEEE Trans. Nucl. Sci.*, vol. 45, no. 6, pp. 2550–2562, Dec. 1998.

[34] R. Garcia, E. J. Daly, H. Evans, P. Nieminen, G. Santin, B. D. Sierawski, and M. H. Mendenhall, "Calibration of the weighed sensitive volume model to heavy ion experimental data," in *Proc. RADECS*, Sep. 19–23, 2011, pp. 60–66.

[35] [Online]. Available: https://creme.isde.vanderbilt.eduon the web at

[36] R. Weller, M. H. Mendenhall, R. A. Reed, R. D. Schrimpf, K. M. Warren, B. D. Sierawski, and L. W. Massengill, "Monte Carlo simulation of single event effects," *IEEE Trans. Nucl. Sci.*, vol. 57, no. 4, pp. 1726–1746, 2010.

[37] K. M. Warren, R. A. Weller, B. D. Sierawski, R. A. Reed, M. H. Mendenhall, R. D. Schrimpf, L. W. Massengill, M. E. Porter, J. D. Wilkinson, K. A. Label, and J. H. Adams, "Application of RADSAFE to model the single event upset response of a 0.25 μm CMOS SRAM," *IEEE Trans. Nucl. Sci.*, vol. 54, no. 4, pp. 898–903, 2007.

[38] T. Bion and J. Bourrieau, "A model for proton-induced SEU," *IEEE Trans. Nucl. Sci.*, vol. 36, no. 6, pp. 2281–2286, Dec. 1989.